Structural Engineering and Mechanics, *Vol. 66, No. 3 (2018) 399-409*
DOI: https://doi.org/10.12989/sem.2018.66.3.399

Response prediction of laced steel-concrete composite beams using machine learning algorithms

Thirumalaiselvi, A.[1*], Mohit Verma[a], Anandavalli, N.[b] and Rajasankar, J.[c]

Academy of Scientific and Innovative Research, CSIR-Structural Engineering Research Centre, CSIR Campus, Taramani, 600 113, Chennai, India

(Received October 31, 2017, Revised February 12, 2018, Accepted February 14, 2018)

Abstract. This paper demonstrates the potential application of machine learning algorithms for approximate prediction of the load and deflection capacities of the novel type of Laced Steel Concrete-Composite[1] (LSCC) beams proposed by Anandavalli *et al*. (Engineering Structures 2012). Initially, global and local responses measured on LSCC beam specimen in an experiment are used to validate nonlinear FE model of the LSCC beams. The data for the machine learning algorithms is then generated using validated FE model for a range of values of the identified sensitive parameters. The performance of four well-known machine learning algorithms, viz., Support Vector Regression (SVR), Minimax Probability Machine Regression (MPMR), Relevance Vector Machine (RVM) and Multigene Genetic Programing (MGGP) for the approximate estimation of the load and deflection capacities are compared in terms of well-defined error indices. Through relative comparison of the estimated values, it is demonstrated that the algorithms explored in the present study provide a good alternative to expensive experimental testing and sophisticated numerical simulation of the response of LSCC beams. The load carrying and displacement capacity of the LSCC was predicted well by MGGP and MPMR, respectively.

Keywords: composite structures; machine learning algorithms; ultimate strength; displacement

1. Introduction

In recent years, effective Steel-Concrete Composite (SCC) structural components are developed for special purpose applications (Liew and Sohel 2009, Yan *et al.* 2014). Mainly, SCC components are used in structures which experience suddenly applied dynamic loads. Those structures should exhibit both enormous ductility and support rotation maintaining the structural integrity. Effective performance of SCC system is mainly based on the composite action achieved by means of shear connectors (Luo *et al.* 2012, Tomlinson *et al.* 1989, Bowerman *et al.* 2002, Liew *et al.* 2009, Leekitwattana, 2011).

Laced Steel-Concrete Composite (LSCC) system is one such SCC system developed by the authors (Anandavalli *et al.* 2012). In LSCC, the top and bottom steel cover plates are connected using lacings and cross-rods as shown in Fig. 1. Lacings transfer the force between steel cover plate and in-filled concrete. Welding is avoided in LSCC by specific arrangement of lacings being tucked into the perforations in the cover plate at suitable places. During experiments under four point bending, LSCC beams found to exhibit large deformation with rotation of about 13° at the supports which is about four times as in the case of Laced Reinforced Concrete components (Anandavalli *et al.* 2012). In addition to this, LSCC system found to possess enormous ductility. Thirumalaiselvi *et al.* (2017) demonstrated the superior blast performance of LSCC. Hence, use of LSSC components is proposed to be extended to other special applications such as concrete based offshore structures, nuclear power plants and blast and impact resistance protective structures. Following certain assumptions, first hand estimation of the LSCC beam capacity has been derived analytically (Thirumalaiselvi *et al.* 2017). However, there is a need to estimate the load and deflection capacities of such a novel system for special applications.

In the current study, Finite Element (FE) analysis is carried out using the general purpose finite element software to obtain the limiting capacity of LSCC beams under monotonic loading. Soil-shell-link approach proposed by (Anandavalli *et al.* 2011) for composite panels has been adopted for the modelling of LSCC beam using appropriate nonlinear material models. The FE model is then validated using the available experimental response of the LSCC beam subjected to monotonic loading. However, FE solutions are found to be computationally expensive for LSCC beams due to their complex geometry. Recently, various researchers have carried out studies towards the development of cost-efficient alternate models based on machine learning algorithms in the different areas of structural engineering-concrete technology (Yan and Shi 2010, Altun *et al.* 2008, Topçu and Sarıdemir 2008, Kumar *et al.* 2013, Toghroli *et al.* 2016, Gajewski *et al.* 2017,

*Corresponding author, Scientist
E-mail: selvi@serc.res.in
[a]Scientist
[b]Principal Scientist
[c]Chief Scientist
[1]US Patent filed-US 20140134395, Indian Patent filed-1886DEL2011

ISSN: 1225-4568 (Print), 1598-6217 (Online)

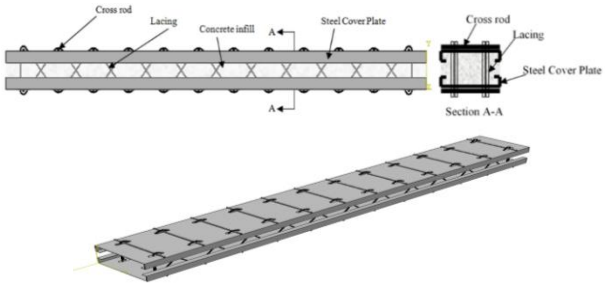

Fig. 1 Isometric view and Cross-section of LSCC system

Parameter	LSCC-45 beam (mm)	LSCC-60 beam (mm)
a	665	670
b	470	610
c	1800	1950

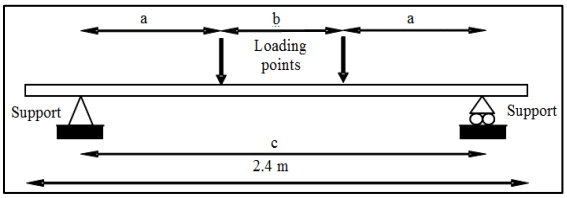

Fig. 2 Loading arrangement on LSCC beam

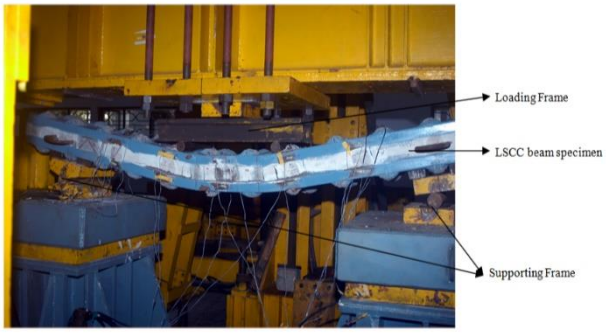

Fig. 3 Test set up

Babanajad *et al.* 2017, Prem *et al.* 2017), fracture mechanics (Yuvaraj *et al.* 2013), materials (Abuomar *et al.* 2015, Bheemreddy *et al.* 2013, Gandomi and Alavi 2012, Verma *et al.* 2017, Prem *et al.* 2018, Singh *et al.* 2018), and geotechnology (Samui 2012, Samui *et al.* 2014, Viswanathan *et al.* 2015, Mozumder *et al.* 2017). In this paper, the popular algorithms like Support Vector Regression (SVR) (Vapnik 2000), Minimax Probability Machine Regression (MPMR) (Strohmann and Grudic 2002), Relevance Vector Machine (RVM) (Tipping 2001) and Multigene Genetic Programing (MGGP) (Searson *et al.* 2010) are chosen to evaluate the displacement and load capacity of LSCC beam. The machine learning algorithms are implemented in the MATLAB software. The training and the testing data for the algorithms are obtained from the validated nonlinear FE model. The relevant input parameters to the algorithms are obtained through parametric study. Based on the parametric study, the inputs which are found to significantly influence the response of the LSCC beam are angle of lacing (LA) and thickness of cover plate (PT). In addition to these two parameters, length

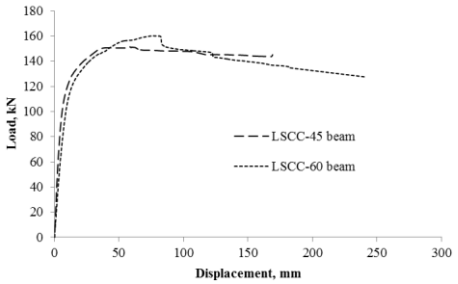

Fig. 4 Load-displacement response of LSCC beams

(L) and width (b) of the LSCC beam are taken as the inputs for the algorithm. The outputs of machine learning algorithm are the ultimate load, failure load, displacement at ultimate and failure loads. The results obtained from the algorithms are found to effectively predict the response of the LSCC beams. Since, the concept of LSCC is new, development of models for prediction of its response will certainly be useful. Further, development of such alternate models gains significance as conventional laboratory experiments cannot be conducted at large deformation range while development of FE model is found to be cost- and time-prohibitive.

2. Experimental investigations

LSCC beam having cross-section of 300 mm×150 mm and length of 2.4 m is chosen for the present study. Cover plates are made of 3 mm thick cold formed steel provided with 50 mm lip on each side. Average yield and ultimate stress of cold formed steel are 210 MPa and 300 MPa. Two beam specimens, one with 45° lacing angle (labelled as LSCC-45) and other with 60° lacing angle (labelled as LSCC-60) are fabricated. The cover plate assembled with lacings and cross rods is shown in Fig. 1. Lacings and cross rods are made of mild steel whose average yield and ultimate stress are found to be 400 MPa and 540 MPa, respectively. Diameter of lacing and cross rod is 8 mm and 10 mm, respectively.

Two-point load test is conducted on both the LSCC beam specimens under displacement control mode. The specimen is loaded at the rate of 0.04 mm/s. The schematics of the loading are shown in Fig. 2. The specimens are tested with simply supported boundary conditions. The actual testing set-up is shown in Fig. 3. For further details about the experiment, the readers are advised to refer (Anandavalli *et al.* 2012). Load displacement of LSCC beams at the mid-point is shown in Fig. 4. During experiment, both the beams were found to possess large deformation and ductility. However, the test was discontinued to avoid the risk of support rod slipping at such large deformation. As the experiment has been stopped abruptly due to safety issues, the ultimate capacity could not be ascertained.

3. Finite element analysis

Thirumalaiselvi *et al.* (2016) explains the detailed finite

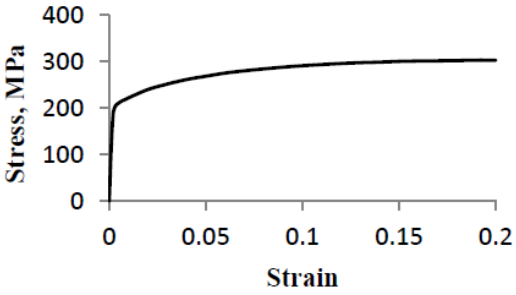

Fig. 5 Stress-strain behaviour of cold-formed steel

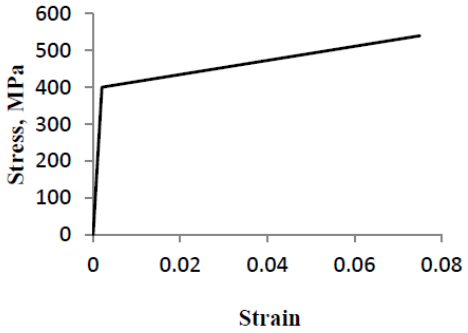

Fig. 6 Stress-strain behaviour of mild steel

element (FE) studies carried out on LSCC beam specimens. However, for the sake of continuity, details about FE analysis will be explained in this section. Solid-shell-link is used to model LSCC system using solid element for concrete core, shell for steel plates and link for shear connectors (Anandavalli *et al.* 2011). Two point loading with simply supported boundary conditions are applied as shown in Fig. 2.

Concrete damaged plasticity (CDP) model is used to represent complete inelastic behaviour of concrete. The stress-strain relationship of concrete and steel is needed for the FE analysis of LSCC beams. Stress-strain relationship of concrete in compression is modelled using empirical relationship given by Attard and Setunge (1996). Pre-cracking tensile stress-strain behaviour is assumed to be linear while post-cracking behaviour in tension is modelled based on the relation proposed by Guo and Zhang (1987). Nonlinear behaviour of steel is modelled using plasticity model available in the software. Material behaviour of steel cover plate is employed based on the nominal stress-strain behaviour of cold formed steel (as shown in Fig. 5). Bi-linear stress-strain behaviour (Fig. 6) is adopted to model the lacings and cross rods.

Surface to surface contact interactions adopting friction formulation in tangential direction (with the coefficient of friction as 0.4) and hard contact in normal direction is used to model the interaction between the steel cover plates and concrete. Contact constraints are enforced using penalty method. Node to surface interaction is given between nodes of crossrods and steel plate. Lacings are connected with cross rods at intersecting nodes and embedded in concrete. The classical coulomb friction model is adopted to characterize the frictional behaviour between the surfaces. Friction is defined as

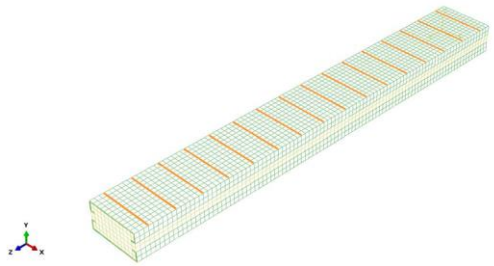

Fig. 7 FE model of LSCC beam

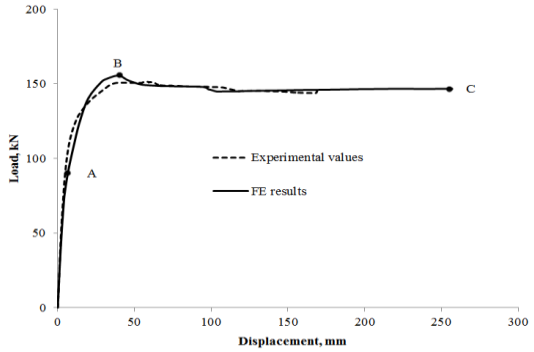

Fig. 8 Load-displacement behaviour of LSCC-45 beam

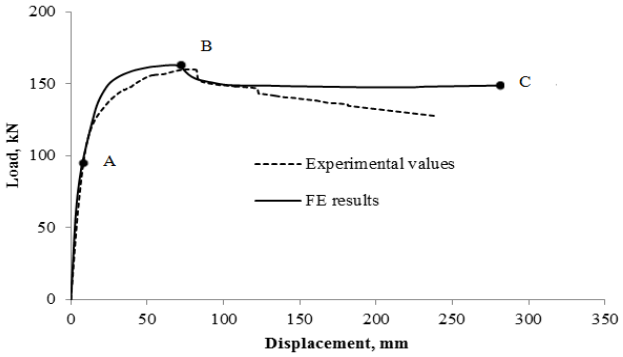

Fig. 9 Load-displacement behaviour of LSCC-60 beam

$$\tau_{tim} = \mu P \quad (1)$$

where τ_{lim} = limiting shear stress, μ = coefficient of friction and P = normal contact pressure.

Convergence study is carried out in arriving at the final FE mesh. The final mesh having elements of size 25 mm with aspect ratio 1 which is shown in Fig. 7 is chosen for the analysis.

The static response of LSCC under four point bending is obtained using nonlinear static analysis. Newton-Raphson solution technique is used. Load-displacement behaviour and critical stages of failure are obtained from the analysis. FE model developed is validated with the results obtained from experiments available in Anandavalli *et al.* (2012). Load-displacement values of LSCC-45 and LSCC-60 beam obtained using FE analysis are shown in Figs. 8 and 9, respectively.

In Figs. 8 and 9, the points A, B, C show the critical stages of loading noticed in FE results. Point A denotes the point at which yielding of bottom cover plate initiated for a tensile strain of 0.0059 in case of LSCC-45 beam and

0.00541 in case of LSCC-60 beam. Ultimate loading stage is denoted by point B. At this stage, crushing of concrete occurs in the compression zone in shear span region for a strain of about 0.0035. In experiment also, similar results were reported. Point C denotes the failure stage. At this stage, strain values in lacings and cross rods are much lesser than its ultimate values. Results obtained using FE model and experiments are found to match well. Hence, the validated FE model is used further in the present study for the generation of wide range of dataset.

4. Background on machine learning algorithms

Machine learning is the computation process of constructing patterns from data. Algorithms based on machine learning are useful where it is difficult to model the complex behaviour of the system or where computational efficiency is the prime requirement. The powerful capabilities of the models based on machine learning can be seen by applying to a simulation where the factors/variables affecting the output are known but the exact relationship between the variables and output is not well known. This section reviews four different machine learning algorithms which are widely used and so adopted in present study.

4.1 Support vector regression (SVR)

SVR is a supervised learning model established by Vapnik (2000) to predict the output (y) for the known input (x). The main principle of SVR is structural risk minimization. The nonlinear SVR problem is written as

$$y = f(x) = \langle w, \phi(x) \rangle + b \tag{2}$$

where w and b represents the function parameters, $\langle , \rangle$ denotes the inner product, and $\phi(x)$ is the transformation. SVR uses a penalty function which predicts the actual values of the target as close as possible with a precision ε. The ε-insensitive penalty function is adopted which is expressed as

$$L_1{}^{\varepsilon}(f(x), y) = \begin{cases} 0 & for\ |f(x) - y| < \varepsilon \\ |f(x) - y| & otherwise \end{cases} \tag{3}$$

Following minimization expression is used by by varying C

$$\Omega = \frac{1}{2}||w||_2^2 + C\sum_{n=1}^{N} L_1^{\varepsilon}(y_n, \langle w, \phi(x_n) \rangle + b) \tag{4}$$

The minimization problem can be written as (Vapnik 2000)

$$\underset{w \in \mathbb{R}^n, b \in \mathbb{R}}{min} ||w||_2^2 + C\sum_{n=1}^{N}\left(\xi_n^2 + \check{\xi}_n^2\right) \tag{5}$$

subject to$(\langle w, \phi(x_n) \rangle + b) - y_n \leq \varepsilon + \check{\xi}_n$,
$y_n - (\langle w, \phi(x_n) \rangle + b) \leq \varepsilon + \xi_n$,
$\xi_n, \check{\xi}_n \geq 0\ n = 1, \ldots, N$
where $\xi_n$and $\check{\xi}_n$represent the upper and lower bounds on output. Method of Lagrange multipliers are used to solve the above mentioned quadratic optimization problem:

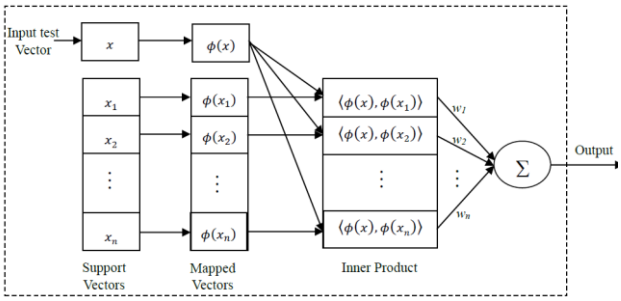

Fig. 10 Graphical representation of SVR

$$f(x) = \sum_{n=1}^{l}(\alpha_n - \check{\alpha}_n)K(x, x_n) - \frac{1}{2}\sum_{n=1}^{l}(\alpha_n - \check{\alpha}_n)[K(x_r, x_n) + K(x_s, x_n)] \tag{6}$$

where α and $\check{\alpha}$ are the Lagrange multipliers, x_r and x_s are two typical support vectors, l is the number of support vectors and K(,) is a kernel function. Presently, radial basis function defined in the following equation is used.

$$K(x, x_n) = \exp\left\{-\frac{(x - x_n)^T(x - x_n)}{2\gamma^2}\right\} \tag{7}$$

The entire process of the proposed model based on SVR is summarised graphically as shown in Fig. 10. The model's performance depends only on the values of the parameters like C, ε and γ which makes the model to be problem-specific. The model is not limited by the number of input variables or any such aspect.

The following observations about SVR are worth noting:

i. Even in the presence of bias, the appropriate selection of the model hyperparameters makes SVR robust.

ii. SVR linearizes by means of kernel function transformation. Hence, the model accuracy is independent of the selection of linearization function.

iii. SVR required tuning of the model parameters and the results obtained are non-probabilistic.

4.2 Relevance vector machine

RVM is based on Bayesian formulation having identical SVR functional form (Tipping 2001). The outputs of RVM can be written as

$$y(x) = \sum_{n=1}^{N} w_n K(x, x_n) + w_0 \tag{8}$$

where w_0 is bias, w_n are the model weights and $K(x, x_n)$ is a kernel function

The likelihood of the dataset assuming $p(t|x)$ as Gaussian $N(t|y(x), \sigma^2)$ is given by (Tipping 2001)

$$p(t|w,\sigma^2) = (2\pi\sigma^2)^{-N/2}\exp\left\{-\frac{1}{2\sigma^2}\|t-\Phi w\|^2\right\} \quad (9)$$

where Φ is the N x (N+1) design matrix with $\Phi_{nm} = K(x_n, x_{m-1})$ with $\Phi_{n1} = 1$, $t = (t_1, \ldots, t_n)$ and $w = (w_0, \ldots, w_n)$. The hyperparameters (α_i) are used for each weight towards avoiding severe over fit issue and providing sparse properties. Applying Bayes' rule, the weights can be evaluated as (Tipping 2001)

$$p(w|t,\alpha,\sigma^2) = (2\pi)^{-\frac{N+1}{2}}|\Sigma|^{-\frac{1}{2}}\exp\left\{-\frac{1}{2}(w-\mu)^T\Sigma^{-1}(w-\mu)\right\} \quad (10)$$

$$\Sigma = (\Phi^T B\Phi + A)^{-1} \text{and } \mu = \Sigma\Phi^T Bt$$

where $A = diag(\alpha_0, \ldots, \alpha_N)$ and $B = \sigma^{-2}I_N$.

The marginal likelihood for the hyperparameters is descried by Tipping (2001)

$$p(t|\alpha,\sigma^2) = (2\pi)^{-\frac{N}{2}}|\mathrm{B}^{-1} + \Phi A^{-1}\Phi^T|^{-\frac{1}{2}}\exp\left\{-\frac{1}{2}t^T(B^{-1} + \Phi A^{-1}\Phi^T)^{-1}t\right\} \quad (11)$$

The values of α and σ^2 maximizing the likelihood of hyperparameters are determined. The salient features of RVM worth noting are:

i. RVM has less sensitivity to the hyperparameters. The output of RVM is probabilistic in nature.

ii. RVM provides sparse models. The sparse model has few relevance vectors which makes interpretation at lesser cost.

iii. RVM is not suitable for larger datasets since training included the highly nonlinear optimization problem.

4.3 Minimax probability machine regression

MPMR was proposed for classification problems by Lanckriet et al. (2003) and was later extended to regression by Strohmann and Grudic (2002).

The aim of the MPMR is to find the hyperplane which distinguishes the two classes. MPMR poses the regression problem as the maximization of the minimum probability of the outputs within some specified bounds of the true regression function. Mathematically, if the hyperplane is assumed to be of the following form

$$a^T z = b, \qquad a, z \in R^n and\ b \in R \quad (12)$$

where R^n is a n-dimensional space, z is random vector, and a, b are constants. The MPMR optimization problem can be written as

$$\max_{\alpha,b,a}\alpha \quad (13)$$

Subject to: $\inf Pr\{a^T x \geq b\} \geq \alpha$

$\inf Pr\{a^T y \leq b\} \geq \alpha$

Lagrangian of the problem is formulated and by substitution of variables the final optimization takes the following form (Lanckriet *et al.* 2003)

$$\min_a \sqrt{a^T\sum\nolimits_x a} + \sqrt{a^T\sum\nolimits_y a} \quad (14)$$

Subject to: $a^T(\bar{x} - \bar{y}) = 1$

where x, y are the random vectors, $\bar{x}, \bar{y}$ are the means and $\sum_x, \sum_y$ are covariance matrices. When the kernel functions are used to map data to higher dimensional space from the original sample space, the transformed optimization problem can be written as (Strohmann and Grudic 2002)

$$\min_\gamma \left\{\left\|\frac{\widetilde{K}_x}{\sqrt{N_x}}\right\|_2 + \left\|\frac{\widetilde{K}_y}{\sqrt{N_y}}\right\|_2\right\} \quad (15)$$

Subject to: $\gamma^T(\tilde{k}_x - \tilde{k}_y) = 1$

$\gamma = \left[\alpha_1\alpha_2 \ldots \alpha_{N_x}\beta_1\beta_2 \ldots \beta_{N_y}\right]^T$

$a = \sum_{i=1}^{N_x}\alpha_i\phi(x_i) + \sum_{i=1}^{N_y}\beta_i\phi(y_i)$

$\widetilde{K}_x = K_x - 1_{N_x}\tilde{k}_x$

$\widetilde{K}_y = K_y - 1_{N_y}\tilde{k}_y$

$\tilde{k}_x, \tilde{k}_y \in R^{N_x+N_y}$ and

$$[\tilde{k}_x]_i = \frac{1}{N_x}\sum_{j=1}^{N_x}K(x_j, z_i), [\tilde{k}_y]_i = \frac{1}{N_y}\sum_{j=1}^{N_y}K(y_j, z_i)$$

$$z_i = \begin{cases} x_i & i = 1,2,\ldots,N_x \\ y_{i-N_x} & i = N_x+1, N_x+2, \ldots, N_x+N_y \end{cases}$$

where $(N_x, N_y)$are the number of points in class (x, y), 1_k is a k-dimensional column vector of ones, $K(z_1, z_2) = \phi(z_1)^T\phi(z_2)$ is a kernel function, K_x contains the first N_x rows of the Gram matrix K (square matrix consisting of the elements $K_{ij} = K(z_i, z_j)$) and K_y contains the first N_y rows of the Gram matrix K. The data is classified into by shifting the regression data to $\pm\epsilon$.

$$u_i = (y_i + \epsilon, x_{i1}, x_{i2}, \ldots, x_{iN})$$
$$v_i = (y_i - \epsilon, x_{i1}, x_{i2}, \ldots, x_{iN}) \quad (16)$$

where N is a number of datasets

Using the above two classes, the classification boundary is obtained by solving the optimization problem described by Eq. (14). The classification boundary is given by

$$\sum_{i=1}^{2N}\gamma_i K(z_i, z) + b = 0 \quad (17)$$

where γ, b are the outputs of the MPMR model.

The following are the important features of MPMR:

i. MPMR model assumes that the mean and co-variance matrix of the distribution that generated the regression data are known. The evaluation of the mean and co-variance statistics directly from the training data results in accurate lower probability bound.

ii. In MPMR also, the solution is unique as it solves convex optimization problem.

4.4 Nonlinear multigene genetic programming

Genetic programming (GP) is a bio-inspired learning

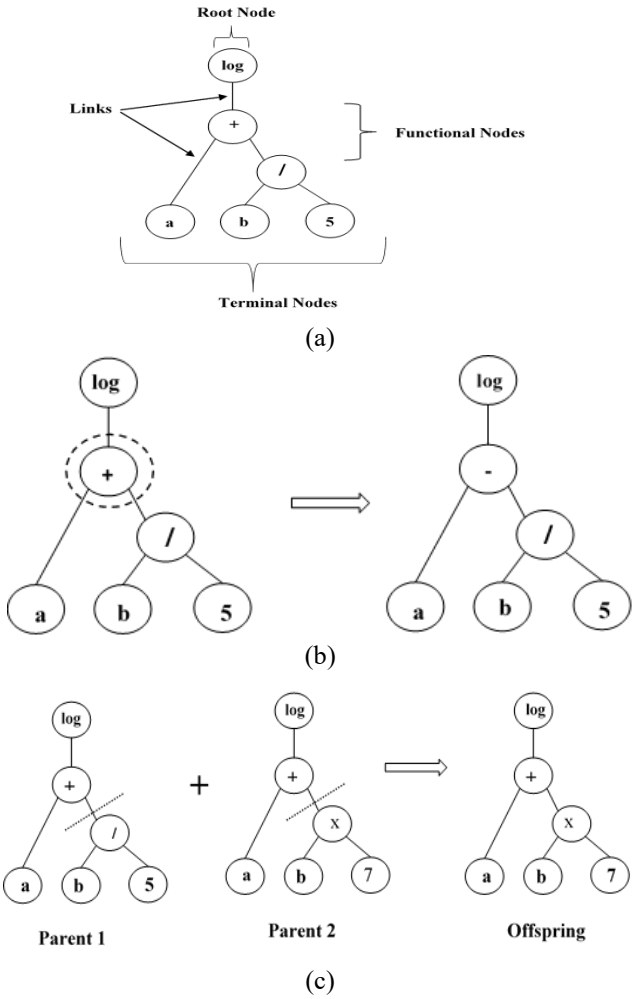

Fig. 11 GP model (Verma *et al.* 2017)-(a) tree structure (log(a+b/5)), (b) mutation and (c) crossover

algorithm which uses the principle of Darwinian natural selection. GP involves the generation of the random population. A typical individual in the population takes the form of a hierarchically structured tree comprising of root, functional and terminal nodes connected by links (Fig. 11). The next step in the GP involves the selection of the individuals for reproduction. A new generation is created by generating new individuals through crossover, mutation and direct reproduction. The process of evolution is continued by computing the fitness of new generation. The output of the GP is the individual with best fitness value in any generation. GP has the ability to predict without assuming any relationship between the input and the output which gives it an edge over other regression and neural network-based methods.

MGGP is a form of symbolic regression carried out using GP. In MGGP, the initial population consists of the random generated GP trees. A mathematical expression is coded in each of the GP tree (Fig. 12). The tree here is analogous to a gene. The tree is then evolved by the process similar to that of GP. The output of MGGP can be viewed as the linear combination of the lower order nonlinear transformations of the input variables. For more details, reader is advised to refer (Gandomi and Alavi 2012,

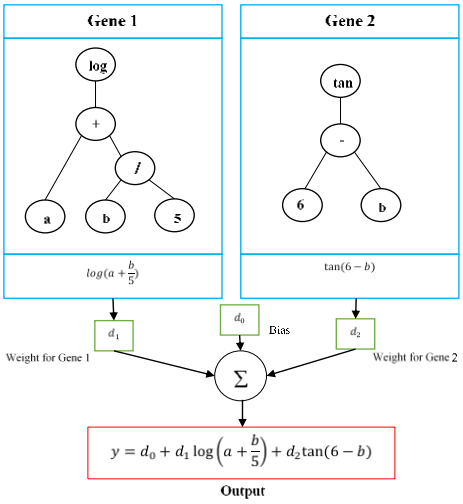

Fig. 12 Multigene GP model (Verma *et al.* 2017)

Searson *et al.* 2010).

The key features of MGGP observed are:

i. The solution obtained from MGGP is not unique. So, the solution corresponds to local minimum.

ii. MGGP is helpful in developing empirical relation between the inputs and the outputs.

5. Data generation

The data is generated for the machine learning algorithms by carrying out FE analysis of the validated model for a range of sensitive parameters. The sensitive parameters which influence the response of LSCC beams were identified by authors in their previous studies (Thirumalaiselvi *et al.* 2016) by carrying out parametric analysis. The sensitive parameters are lacing angle (LA), cover plate thickness (PT), width (b) and length (L) of the beam. The depth of the beam could be another parameter which can influence the response of LSCC. Similar to the case of conventional RC beam, the depth of LSCC is directly proportional to the load and inversely to displacement capacity. Since the relationship is well known, the depth is kept at a constant value of 150 mm keeping in view the objective of the present study. The results of the FE analysis are given in Table 1 for different configurations of LSCC beams

6. Model applications

The models described in section 3 are used for predicting the load and displacement at ultimate and failure stages of LSCC for different configurations. The following relationships are assumed

$$\left.\begin{matrix} P_u \\ P_f \\ \Delta_u \\ \Delta_f \end{matrix}\right\} = f(LA, b, L, PT) \tag{18}$$

Table 1 Numerically predicted responses of LSCC beams

SNo	Inputs				Outputs			
	LA (°)	b (mm)	L (mm)	PT (mm)	Pu(kN)	Pf (kN)	Δu (mm)	Δf(mm)
Training dataset								
1	30	300	2400	2	99.3	89.11	111.018	279.5
2	30	300	2400	4	167.67	151.1	84.5	260.67
3	30	300	2400	5	202.8	189.7	89.285	303.17
4	30	400	2400	3	169.3	158.65	115.8	200.12
5	30	400	2400	5	256	240.76	114.6	308.4
6	30	300	1800	4	223.5	206	59.3	218.6
7	30	400	1800	3	226.24	209.29	74.5	157.58
8	30	400	1800	4	282.5	261.4	80.83	216.73
9	30	400	1800	5	327.15	313.66	127.48	295.2
10	30	300	1500	4	262.55	245.62	66.08	156.81
11	45	300	2400	2	97.2	87.67	143.51	214.73
12	45	300	2400	4	167.94	158.42	90.61	173.83
13	45	300	2400	5	204.32	191.14	89.87	209.08
14	45	400	2400	3	167.05	155.45	137.22	207.2
15	45	400	2400	4	211.06	199.12	98.34	192.9
16	45	300	1800	2	129.53	118.28	91.62	144
17	45	300	1800	3	176.98	165.9	61.53	130.53
18	45	300	1800	5	271.55	257.75	64.09	184.45
19	45	400	1800	3	223.32	208.46	87.9	138.64
20	45	300	1500	2	155.5	120.8	68.3	105.4
21	45	300	1500	3	211.81	198.9	40.28	106.53
22	45	400	1500	3	268.1	251.34	61.66	102.26
23	60	300	2400	2	97.15	97.06	259.56	274.493
24	60	300	2400	4	169.9	162.75	108.88	210.66
25	60	400	2400	2	121.27	121.05	206.01	229
26	60	400	2400	4	214.65	202.4	137.3	213.8
27	60	400	2400	5	259.35	249.12	107.5	210.6
28	60	300	1800	2	129.34	127.9	144.36	163.03
29	60	300	1800	4	226.15	217.35	60.77	127.066
30	60	300	1800	5	274.28	267.67	60.72	145.59
31	60	400	1800	4	285.86	271.9	79.2	130.35
32	60	400	1800	5	344.49	329.92	70.2	166.56
33	60	300	1500	2	214.3	146.2	56.46	87.7
34	60	400	1500	3	269.6	251.9	76.14	108.43
35	60	400	1500	5	399.06	388.34	91.24	203.68
Testing dataset								
36	30	300	2400	3	133.3	121.1	87.37	257.8
37	30	400	2400	2	125	116.6	159.5	224.13
38	30	400	2400	4	212.5	198.8	95.9	235.5
39	30	300	1800	2	133.3	117.4	70.16	200.72
40	30	300	1800	3	177.5	160.8	52.26	191.9
41	30	300	1800	5	262.3	249	78.2	297.77
42	30	300	1500	3	213.2	193.44	41.5	130.4
43	45	300	2400	3	132.6	122.63	96.67	177.03
44	45	400	2400	2	121.64	119.3	158.94	244.7
45	45	400	2400	5	255.57	239.37	95.28	242.3
46	45	300	1500	4	267.27	250.78	46.73	142.5
47	45	400	1500	4	336.2	317.76	60.57	144.77
48	45	300	1800	4	223.94	211.88	51.7	121
49	45	400	1800	4	281.5	267.76	66.33	133.53
50	60	300	2400	3	133.91	126.67	125.55	186.67
51	60	300	2400	5	206.9	201.33	97.69	216.3
52	60	400	2400	3	168.72	159	174	218.23
53	60	300	1800	3	178.17	167.92	72.49	117.77
54	60	400	1800	3	224.62	209.67	101.09	145.69
55	60	300	1500	3	154.3	199.97	76.62	106.69

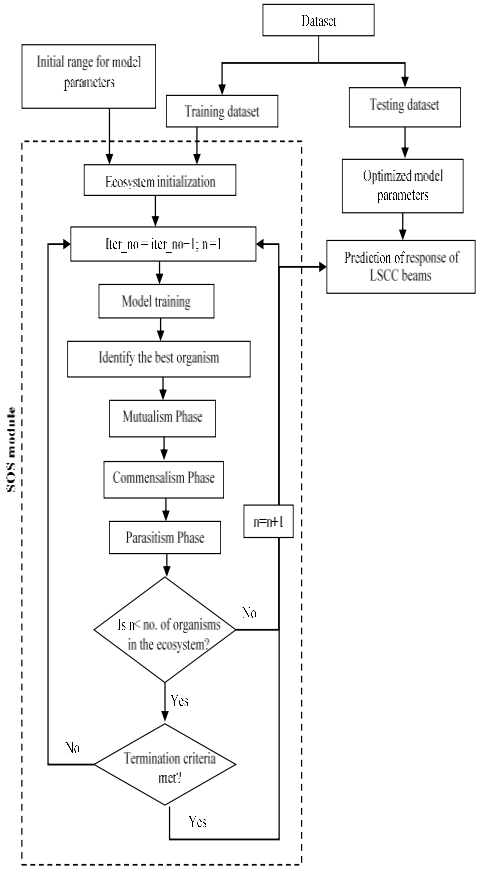

Fig. 13 Flow chart for hyperparameters optimization using SOS (Verma *et al.* 2017)

The dataset obtained from the FE simulations is used for developing models based on machine learning using different algorithms. Out of 55 datasets, 35 are used for training while 20 are used for testing the model. The dataset is normalized to have a value between 0 and 1. Since machine learning algorithms are applied for the first time to predict the response of LSCC beam, the basis for the selection of the parameters is not available in the literature. In such situations, an independent optimization problem with model parameters as the design variables should be solved. In the present study, Symbiotic Organism Search

Table 2 Parameters used in SVR

Parameter	Values			
	P_u	P_f	Δ_u	Δ_f
Loss function	Quadratic	Quadratic	Quadratic	Quadratic
Kernel function $K(x_i,x)$	Radial basis function $e^{-\frac{(x_i-x)^T(x_i-x)}{2\gamma^2}}$	Radial basis function $e^{-\frac{(x_i-x)^T(x_i-x)}{2\gamma^2}}$	Radial basis function $e^{-\frac{(x_i-x)^T(x_i-x)}{2\gamma^2}}$	Radial basis function $e^{-\frac{(x_i-x)^T(x_i-x)}{2\gamma^2}}$
C	50	1100	2200	1100
γ	2.8	3	3.2	1

Table 3 Parameters used in RVM

Parameter	Values			
	P_u	P_f	Δ_u	Δ_f
Kernel function $K(x_i,x)$	Radial basis function $e^{-\frac{(x_i-x)^T(x_i-x)}{2\gamma^2}}$	Radial basis function $e^{-\frac{(x_i-x)^T(x_i-x)}{2\gamma^2}}$	Cubic $(\gamma((x_i-x)^T(x_i-x))^{\frac{2}{3}}$	Laplace $e^{-\frac{(x_i-x)^T(x_i-x)}{\gamma}}$
γ	2.3	2.3	2	5

Table 4 Parameters used in MPMR

Parameter	Values
	$P_u, P_f, \Delta_u, \Delta_f$
Kernal function $K(x_i,x)$	Polynomial $(x_i x^T+1)^{p_1}$
p_1	2
ϵ	0.0055

Table 5 Parameters used in MGGP

Parameter	Values
	$P_u, P_f, \Delta_u, \Delta_f$
Function set	x,+,-,tanh,sin,cos,exp
Population size	200
Number of generation	200
Maximum number of genes	2
Maximum tree depth	5
Tournament size	3
Elitism	0.05
Crossover events	0.85
Mutation events	0.1
Direct reproduction	0.05
Ephemeral random constants	[-10 10]

(SOS) algorithm which was developed by Cheng and Prayogo (2014) is used for optimization of the model parameters. The objective function is taken as the maximization of the coefficient of determination (R^2) for the training dataset. The flow chart for the procedure followed is shown in Fig. 13. The values of the parameters obtained are given in Tables 2 to 5 for different algorithms. Out of the four machine learning algorithms, MGGP is the only one which gives an explicit relation between the inputs and the outputs in the form of a mathematical expression. The expressions obtained for P_u, P_f, Δ_u and Δ_f using MGGP are given in Table 6. These expressions hold good, when the values of input parameters are chosen within the range taken in the present study. The outputs obtained from different models are compared with Finite Element Method (FEM) results in Figs. 14 and 15 for training and testing datasets, respectively.

Table 6 Mathematical expression obtained for LSCC responses using MGGP

Response parameter	Mathematical expression
P_u	$0.53PT - 0.09L - 0.17\tanh(\tanh(L)) + 0.09b.L - 0.17L.PT - 0.11\cos\big((L-1.05)(LA-L)\big)e^{\cos(b)} + 0.49$
P_f	$0.18b + 0.17e^{PT} + 0.17\tanh(PT) + 0.04PT(LA+e^b+1.91) - 0.07\sin\big(\sin(L)(PT+e^b+2e^{PT})\big) - 0.003$
Δ_u	$0.17\tanh\big(b - PT + \tanh(L)(L-PT)\big) - 0.29\cos(LA-2PT+\tanh(L)) + 0.2\cos(b)\tanh(L)(e^{LA}+\tanh(b)) + 0.3$
Δ_f	$0.09(LA+b.PT)(\cos(LA)+b.PT) - 1.49e^{\tanh(LA+\cos(PT))} + 0.2\cos(PT)(3.9L-\sin(L)) - 0.2e^{\sin(L)}(0.25b+\tanh(PT)) + 0.08LA(L+PT+6.47) + 3.41$

Table 7 Error indices for training dataset

Algori-thm	R^2				RMSE				MAPE			
	P_u	P_f	Δ_u	Δ_f	P_u	P_f	Δ_u	Δ_f	P_u	P_f	Δ_u	Δ_f
SVR	0.982	0.989	0.849	0.866	9.630	7.383	17.465	22.458	0.0335	0.0286	0.1332	0.0935
RVM	0.978	0.993	0.802	0.813	10.388	5.763	19.215	25.863	0.0333	0.024	0.1607	0.1168
MPMR	0.990	0.997	0.932	0.945	7.096	3.824	11.209	14.039	0.0217	0.0161	0.0854	0.0666
MGGP	0.982	0.994	0.933	0.897	9.424	5.216	11.148	19.158	0.0279	0.0231	0.0832	0.0798

Table 8 Error indices for testing dataset

Algori-thm	R^2				RMSE				MAPE			
	P_u	P_f	Δ_u	Δ_f	P_u	P_f	Δ_u	Δ_f	P_u	P_f	Δ_u	Δ_f
SVR	0.926	0.987	0.811	0.691	16.794	6.395	17.350	29.662	0.047	0.025	0.1598	0.1313
RVM	0.938	0.992	0.750	0.789	15.632	5.135	19.640	24.569	0.0507	0.0237	0.1875	0.1006
MPMR	0.910	0.991	0.846	0.831	18.390	5.547	15.723	22.509	0.0459	0.0258	0.1298	0.1093
MGGP	0.946	0.995	0.780	0.745	14.342	4.149	18.399	27.479	0.0418	0.0202	0.1552	0.1294

7. Discussion and inferences

In this section, the error indices are defined in order to quantify the accuracy of the algorithms, followed by discussion and inferences drawn.

7.1 Error indices

In order to quantify the performance of various machine learning algorithms, following error indices are defined:

i. Coefficient of determination (R^2)

$$R^2 = \frac{\sum_{i=1}^{n}(y_i-\bar{y})^2(x_i-\bar{x})^2}{\sum_{i=1}^{n}(x_i-\bar{x})(y_i-\bar{y})} \tag{19}$$

ii. Root mean square of percentage error (RMSE)

$$RMSE = \sqrt{\frac{1}{n}\sum_{i=1}^{n}(y_i-x_i)^2} \tag{20}$$

iii. Mean absolute percentage error (MAPE)

$$MAPE = \frac{1}{n}\sum_{i=1}^{n}\left|\frac{x_i-y_i}{y_i}\right| \tag{21}$$

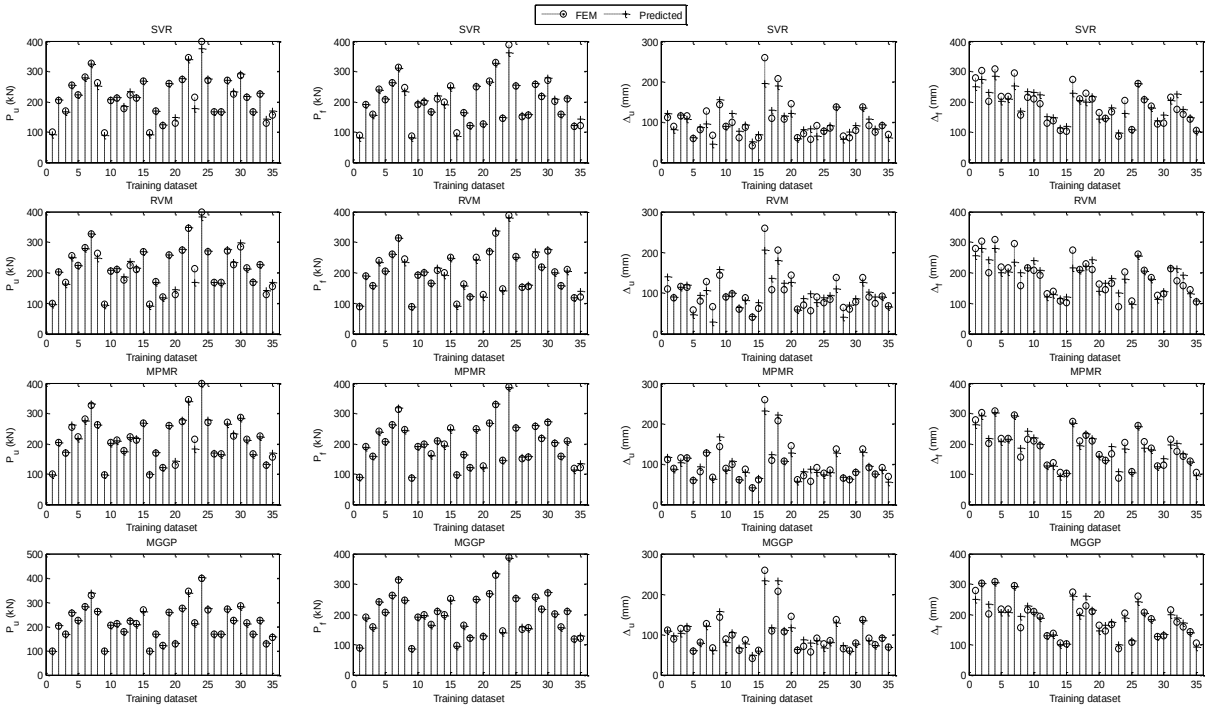

Fig. 14 Comparison of FEM and predicted responses for training dataset

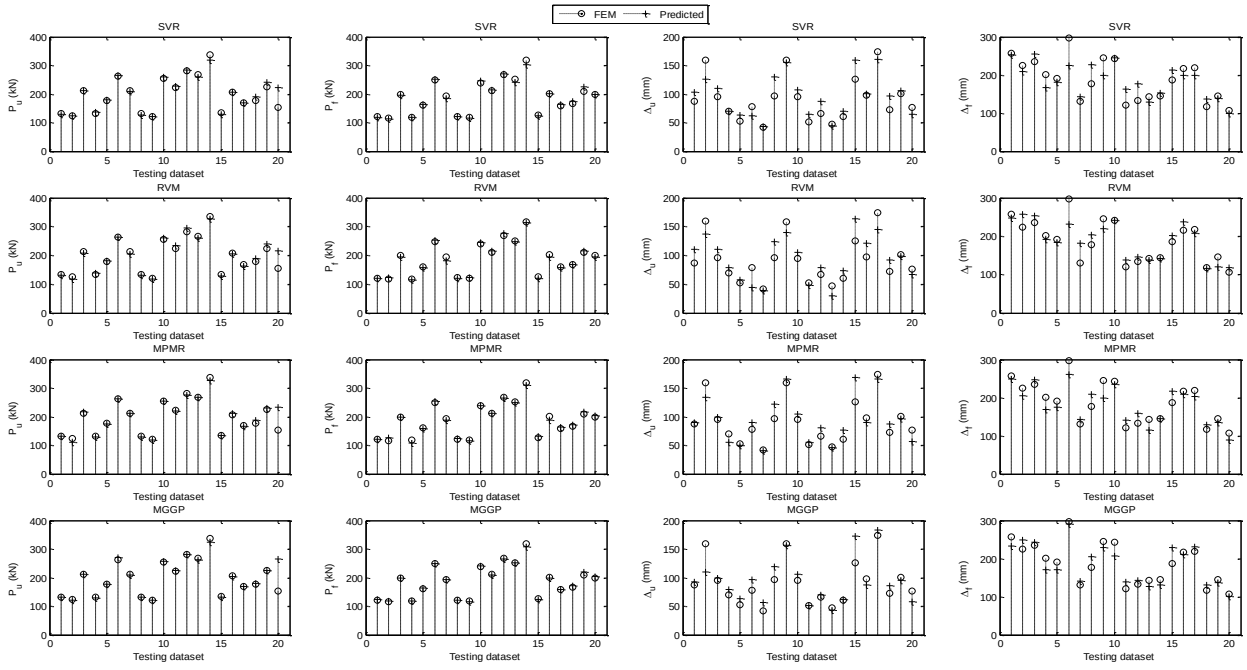

Fig. 15 Comparison of FEM and predicted responses for testing dataset

where y, x are the FEM and predicted values.

The R^2, RMSE and MAPE evaluated are shown in Tables 7 and 8.

7.2 Discussion

Based on the values of error indices, in general all the four methods are found to perform well for the response prediction of the LSCC beam. In the training phase, the values of the RMSE and MAPE for (P_u, P_f, Δ_f) are found to be least for MPMR. In case of Δ_u, RMSE and MAPE are found to be least for MGGP. Similarly, the R^2 values are found to be highest for MPMR in case of (P_u, P_f, Δ_f) and MGGP in case of Δ_u. In the testing phase, the values of RMSE and MAPE are found to be least for MGGP for predicting of (P_u, P_f) and MPMR for predicting (Δ_u, Δ_f). The R^2 values are found to be on the higher side for MGGP in case of (P_u, P_f) and MPMR in case of(Δ_u, Δ_f). Some

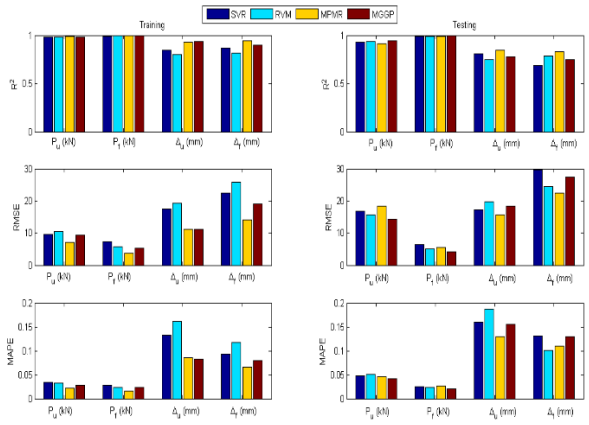

Fig. 16 Comparison between models in terms of error indices for training and testing data

model tends to over fit the training data and shows good performance in the training phase. Therefore, the conclusions in the present study are drawn from the error indices values in the testing phase. Based on the values of error indices obtained in the testing phase, it is suggested to use MGGP for predicting (P_u, P_f) and MPMR for predicting (Δ_u, Δ_f).

7.3 Inferences

Following inferences are drawn from the present study:

a. Principle-SVR works on the principle of structural risk minimization (SVR) which minimizes upper bound on the expected risk. RVM is identical to SVR in functional form. RVM assumes sparse distribution of the weights. MPMR works on the principle of maximization of the minimum probability of the outputs within specified bounds of the true regression function. MGGP uses to symbolic regression based on GP.

b. Uniqueness of the solution-SVR, RVM and MPMR solves a convex optimization problem. Therefore, the solution obtained is always unique and global minimum. MGGP does not provide unique solution. The solution corresponds to the local minimum.

c. Computational efficiency-RVM provides sparse models with fewer relevance vectors. This makes the interpretation lesser computationally intensive. However, a nonlinear optimization is carried out in the training phase of RVM which makes it unsuitable for large data.

d. Probabilistic nature-Results obtained from SVR and MGGP are not probabilistic in nature. MPMR and RVM incorporate the probabilistic nature of the outputs.

8. Conclusions

The response evaluation capability of four different machine learning algorithms, viz., Support Vector Regression (SVR), Minimax Probability Machine Regression (MPMR) Relevance Vector Machine (RVM) and Multigene Genetic Programming (MGGP), for the new type of laced steel-concrete composite (LSCC) beam has been investigated in the present study. Finite Element (FE) model for the LSCC beam has been developed using solid-shell-link approach. The FE model is then validated with experiments of LSCC subjected to monotonic loading. The FE simulations have been carried out over a range of sensitive parameters. The results obtained from the simulations have been used as the training and testing dataset for the machine learning algorithms. The performance of the different machine learning algorithms is assessed in terms of error indices.

The following conclusions are drawn from the present investigations:

i. FE analysis-In order to generate data for machine learning algorithms, FE analysis is carried out. Model based on FEM is found to provide better insight into realistic behaviour of LSCC beams (including yielding of cover plates, crushing of concrete). The results obtained from analysis of LSCC model subjected to monotonic loading compared well with those of experiments. The validated FE model is used further in the present study for the generation of wide range of dataset.

ii. Application of machine learning algorithms-SVR, RVM, MPMR and MGGP are compared in terms error indices. MGGP is found to perform well for the prediction of the ultimate and failure loads in terms of R2, RMSE and MAPE. MPMR is found to perform better than other algorithms in the prediction of the displacement at the ultimate and failure load. However, error indices should not be given top priority towards selection of machine learning algorithm. The computational cost associated with the optimization and large storage space demand must be considered as a criteria for some of the practical applications.

Finally, it should be noted that for the modeling of LSCC components FE analysis procedure is generally used. However, FE solutions are found to be computationally expensive for LSCC beams. Hence, towards the development of cost-efficient alternate models, different machine learning algorithms are adopted. Ductility which is the key parameter in blast and impact resistant design of structures can be obtained from the predicted values of displacements through machine learning algorithms.

Acknowledgments

The authors acknowledge the help received from Mr. S. Rajkumar in formatting the final version of the manuscript.

References

Abuomar, O., Nouranian, S., King, R., Ricks, T.M. and Lacy, T. E. (2015), "Comprehensive mechanical property classification of vapor-grown carbon nanofiber/vinyl ester nanocomposites using support vector machines", *Comput. Mater. Sci.*, **99**, 316-325.

Altun, F., Kişi, Ö. and Aydin, K. (2008), "Predicting the compressive strength of steel fiber added lightweight concrete using neural network", *Comput. Mater. Sci.*, **42**(2), 259-265.

Anandavalli, N., Lakshmanan, N., Iyer, N.R., Samuel Knight, G.M. and Rajasankar, J. (2011), "A novel modelling technique for blast analysis of steel-concrete composite panels", *Proc.*

Eng., **14**, 2429-2437.
Anandavalli, N., Lakshmanan, N., Samuel Knight, G.M., Iyer, N.R. and Rajasankar, J. (2012), "Performance of laced steel-concrete composite (LSCC) beams under monotonic loading", *Eng*. *Struct*., **41**, 177-185.
Attard, M.M. and Setunge, S. (1996), "The stress-strain relationship of confined and unconfined concrete", *ACI Mater*. *J*., **93**(5), 432-442.
Babanajad, S.K., Gandomi, A.H. and Alavi, A.H. (2017), "New prediction models for concrete ultimate strength under true-triaxial stress states: An evolutionary approach", *Adv*. *Eng*. *Softw*., **110**, 55-68.
Bheemreddy, V., Chandrashekhara, K., Dharani, L.R. and Hilmas, G.E. (2013), "Modeling of fiber pull-out in continuous fiber reinforced ceramic composites using finite element method and artificial neural networks", *Comput*. *Mater*. *Sci*., **79**, 663-673.
Bowerman, H., Coyle, N. and Chapman, J.C. (2002), "An innovative steel-concrete construction system", *Struct*. *Eng*., **80**(20), 33-38.
Cheng, M.Y. and Prayogo, D. (2014), "Symbiotic organisms Search: A new metaheuristic optimization algorithm", *Comput*. *Struct*., **139**, 98-112.
Gajewski, J., Golewski, P. and Sadowski, T. (2017), "Geometry optimization of a thin-walled element for an air structure using hybrid system integrating artificial neural network and finite element method", *Compos*. *Struct*., **159**, 589-599.
Gandomi, A.H. and Alavi, A.H. (2012), "A new multigene genetic programming approach to nonlinear system modeling. Part I: Materials and structural engineering problems", *Neur*. *Comput*. *Appl*., **21**(1), 171-187.
Guo, Z. and Zang, X. (1987), "Investigation of complete stress-deformation curves for concrete in tension", *ACI J*., **82**(3), 310-24.
Kumar, M., Mittal, M. and Samui, P. (2013), "Performance assessment of genetic programming (GP) and minimax probability machine regression (MPMR) for prediction of seismic ultrasonic attenuation", *Earthq*. *Sci*., **26**(2), 147-150.
Lanckriet, G.R., Ghaoui, L.E., Bhattacharyya, C. and Jordan, M.I. (2002), "A robust minimax approach to classification", *J*. *Mach*. *Learn*. *Res*., **3**, 555-582.
Leekitwattana, M. (2011), "Analysis of an alternative topology for steel-concrete-steel sandwich beams incorporating inclined shear connectors", Ph.D. Dissertation, University of Southampton, Southampton, U.K.
Liew, J.R., Sohel, K.M.A. and Koh, C.G. (2009), "Impact tests on steel-concrete-steel sandwich beams with lightweight concrete core", *Eng*. *Struct*., **31**(9), 2045-2059.
Liew, J.Y.R. and Sohel, K.M.A. (2009), "Lightweight steel-concrete-steel sandwich system with J-hook connectors", *Eng*. *Struct*., **31**(5), 1166-1178.
Luo, Y., Li, A. and Kand, Z. (2012), "Parametric study of bonded steel-concrete composite beams by using finite element analysis", *Eng*. *Struct*., **34**, 40-51.
Mozumder, R.A., Laskar, A.I. and Hussain, M. (2017), "Empirical approach for strength prediction of geopolymer stabilized clayey soil using support vector machines", *Constr*. *Build*. *Mater*., **132**, 412-424.
Prem, P.R., Murthy, A.R. and Verma, M. (2018), "Theoretical modelling and acoustic emission monitoring of RC beams strengthened with UHPC", *Constr*. *Build*. *Mater*., **158**, 670-682.
Prem, P.R., Verma, M., Murthy, A.R., Rajasankar, J. and Bharatkumar, B.H. (2017), "Numerical and theoretical modelling of low velocity impact on UHPC panels", *Struct*. *Eng*. *Mech*., **63**(2), 207-215.
Samui, P. (2012), "Application of relevance vector machine for prediction of ultimate capacity of driven piles in cohesionless soils", *Geotech*. *Geolog*. *Eng*., **30**(5), 1261-1270.
Samui, P., Hariharan, R. and Karthikeyan, J. (2014), "Determination of stability of slope using Minimax Probability Machine", *Georisk*: *Assess*. *Manage*. *Risk Eng*. *Syst*. *Geohaz*., **8**(2), 147-151.
Searson, D.P., Leahy, D.E. and Willis, M.J. (2010), "GPTIPS: An open source genetic programming toolbox for multigene symbolic regression", *Proceedings of the International Multiconference of Engineers and Computer Scientists*, Hong Kong, March.
Singh, D., Maheshwari, S., Zaman, M. and Commuri, S. (2018), "Kernel machines and firefly algorithm based dynamic modulus prediction model for asphalt mixes considering aggregate morphology", *Constr*. *Build*. *Mater*., **159**, 408-416.
Strohmann, T. and Grudic, G.Z. (2002), "A formulation for minimax probability machine regression", *Proceedings of the Advances in Neural Information Processing Systems,* Vancouver, Canada, December.
Thirumalaiselvi, A., Anandavalli, N., and Rajasankar, J. (2017), "Mechanics based analytical approaches to predict nonlinear behaviour of LSCC beams", *Struct*. *Eng*. *Mech*., **64**(3), 311-321.
Thirumalaiselvi, A., Anandavalli, N., Rajasankar, J. and Iyer, N.R. (2015), "Blast response studies on laced steel-concrete composite (LSCC) slabs", *Proceedings of the Advances in Structural Engineering*, New Delhi, India, December.
Thirumalaiselvi, A., Anandavalli, N., Rajasankar, J. and Iyer, N.R. (2016), "Numerical evaluation of deformation capacity of Laced steel-concrete composite beams", *Steel Compos*. *Struct*., **20**(1), 167-184.
Tipping, M.E. (2001), "Sparse Bayesian learning and the relevance vector machine", *J*. *Mach*. *Learn*. *Res*., **1**, 211-244.
Toghroli, A., Suhatril, M., Ibrahim, Z., Safa, M., Shariati, M. and Shamshirband, S. (2016), "Potential of soft computing approach for evaluating the factors affecting the capacity of steel-concrete composite beam", *J*. *Intellig*. *Manufact*.
Tomlinson, M., Tomlinson, A., Chapman, M.L., Jefferson, A.D. and Wright, H.D. (1989), "Shell composite construction for shallow draft immersed tube tunnels", *Proceedings of the ICE International Conference on Immersed Tube Tunnel Techniques*, Manchester, U.K., April.
Topçu, İ.B. and Sarıdemir, M. (2008), "Prediction of mechanical properties of recycled aggregate concretes containing silica fume using artificial neural networks and fuzzy logic", *Comput*. *Mater*. *Sci*., **42**(1), 74-82.
Vapnik, V. (2000), *The Nature of Statistical Learning Theory*, Springer Science & Business Media, New York, U.S.A.
Verma, M., Thirumalaiselvi, A. and Rajasankar, J. (2017), "Kernel-based models for prediction of cement compressive strength" *Neur*. *Comput*. *Appl*., **28**(1), 1083-1100.
Viswanathan, R., Jagan, J., Samui, P. and Porchelvan, P. (2015), "Spatial variability of rock depth using simple kriging, ordinary kriging, RVM and MPMR", *Geotech*. *Geolog*. *Eng*., **33**(1), 69-78.
Yan, J.B., Liew, J.R., Sohel, K.M.A. and Zhang, M.H. (2014), "Push-out tests on J-hook connectors in steel-concrete-steel sandwich structure", *Mater*. *Struct*., **47**(10), 1693-1714.
Yan, K. and Shi, C. (2010), "Prediction of elastic modulus of normal and high strength concrete by support vector machine", *Constr*. *Build*. *Mater*., **24**(8), 1479-1485.
Yuvaraj, P., Murthy, A.R., Iyer, N.R., Sekar, S.K. and Samui, P. (2013), "Support vector regression based models to predict fracture characteristics of high strength and ultra high strength concrete beams", *Eng*. *Fract*. *Mech*., **98**, 29-43.

CC